INTERNATIONAL JOURNAL FOR NUMERICAL METHODS IN FLUIDS, VOL. 9, 151–165 (1989)

NUMERICAL ANALYSIS OF THE DEVELOPING FLUID FLOW IN A CIRCULAR DUCT ROTATING STEADILY ABOUT A PARALLEL AXIS

D. T. GETHIN AND A. R. JOHNSON

Department of Mechanical Engineering, Singleton Park, Swansea SA3 5BE, U.K.

SUMMARY

A numerical analysis of the flow pattern in the inlet region of a circular pipe rotating steadily about an axis parallel to its own is presented. Both finite cell and finite element methods are used to analyse the problem and they give qualitatively similar results which show that a swirling fluid motion is induced in the pipe inlet region. The analyses show that the direction of swirl is opposite to that of the pipe rotation when viewed along the flow axis and that its magnitude depends on the speed of pipe rotation and throughflow Reynolds number. Neither numerical analysis predicts the marked upturn in friction factor (or pressure drop) which has been observed experimentally. However, a dependence on the pipe inlet boundary conditions is demonstrated.

KEY WORDS Numerical analysis Fluid flow Rotating circular duct Finite cell method Finite element method Swirl Inlet boundary conditions

INTRODUCTION

Coolant passages are used extensively in highly rated power-generating machines where there is a requirement to remove heat to ensure reliable long-term operation. As explained in detail by Marlow,[1] they are used in turbogenerators for cooling both stator and rotor windings to prevent insulation breakdown. Alternatively, in the high-temperature stage of a gas turbine they are used to prevent premature blade failure due to the combination of high thermal loading and centrifugal stressing, which is explained by Morris.[2] In the turbogenerator application ducts of different sectional shape are designed into the rotor windings and therefore their axes are aligned with that of rotation. Conversely, in the gas turbine the coolant passages are configured to have their axes normal to that of rotation. For each machine type the overall coolant circuit comprises duct sections which are connected by means of bends, plenums and sealed units between rotating and stationary elemnts; consequently the flow is complex.

It is well known that in ducted flow the heat removed by the coolant depends on its mass flow rate. The latter is dictated by the choice of coolant circulating pump which induces flow around the circuit against the various component resistances. Under stationary conditions the pressure losses in the network are not straightforward to calculate; however, where rotation is present they can be calculated with even less certainty. An indication of the effect of rotation on pressure drop in developing flow in a plain circular duct has been given by Johnson and Morris[3] for flow rates corresponding to laminar through to turbulent flow. This work presented strong evidence to suggest that the effect of rotation is most significant in the developing flow region, where for the

0271–2091/89/020151–15$07.50

Received 8 July 1987
Revised 29 April 1988

range of rotational Reynolds numbers (J) investigated the friction factor was observed to increase up to fourfold depending on the nature of flow conditioning fitted at the pipe entrance. However, under developed flow conditions rotation appeared to have little or no effect on pressure drop. This evidence supports the argument put forward by Morris[4] in which he showed that for the flow configuration under consideration vorticity is generated in the duct plane under conditions of developing flow only. This suggests that same form of swirling flow will occur in this part of the duct, so before the mechanism of heat transfer in this part of the duct is considered, it is essential that some understanding of the flow field is obtained first.

Hitherto, little analysis of developing isothermal flow in a tube rotating about a parallel axis has been undertaken. Driven by industrial requirements, some analysis of flow with heat transfer has been considered, but this has been confined mainly to conditions where the flow approximates to being fully developed. Results from work presented by Woods and Morris,[5] Mori and Nakayama[6] and Skiadaressis and Spalding[7] show that a pair of counter-rotating eddies are induced by density variations across the pipe section. These analyses are based on a boundary layer approach and in the latter[7] developing flow was considered. However, to retain computational simplicity, the shear stress associated with the streamwise velocity gradient was ignored; this renders the flow parabolic in nature which results in computational simplification and economy.

Axisymmetric swirling flow has also been the subject of theoretical and experimental investigation. One of the earliest studies was carried out by Talbot,[8] who performed a perturbation analysis on laminar swirling flow to determine the onset of instability. His prediction was also verified by experimental observation using a dye to facilitate flow visualization. Recently, further investigations of turbulent swirling flows have been carried out. For example, Sparrow and Chaboki[9] presented experimental results for turbulent swirling flows and ultimately observed their influence on the duct friction factor and heat transfer. It was clear that the duct friction factor was increased significantly (up to twenty-fold) over that for fully developed flow. These increases were evident where the swirling motion was most vigorous.

As mentioned above, numerical solutions have been obtained for the governing equations and hitherto these have been based mainly on the approach pioneered by Spalding.[10] During the last decade, however, the finite element method has been applied to the analysis of fluid flow, and its development parallels that of the finite difference approach. Early solutions for two-dimensional flows were based on streamfunction–vorticity statements of the governing equations as explained by Taylor and Hood.[11] The approach was then extended to yield results for primitive variables (velocities/pressure) as described in Reference 12, and currently it is being used for analysing turbulent flows and developing turbulence models.[13]

The object of the present investigation is to examine numerically the laminar developing flow in a circular duct rotating steadily about a parallel axis. Both finite difference and finite element methodologies are used.

GOVERNING EQUATIONS AND THEIR SOLUTION

The equations which may be used to describe fluid flow are the Navier–Stokes equations.[14] They express the principles of conservation of momentum for a control volume in a fluid domain. With reference to Figure 1, for a Cartesian co-ordinate system the governing equations may be written

$$\frac{Du}{Dt} = F_x - \frac{1}{\rho}\frac{\partial p}{\partial x} + \nu\nabla^2 u, \tag{1}$$

$$\frac{Dv}{Dt} = F_y - \frac{1}{\rho}\frac{\partial p}{\partial y} + \nu\nabla^2 v, \tag{2}$$

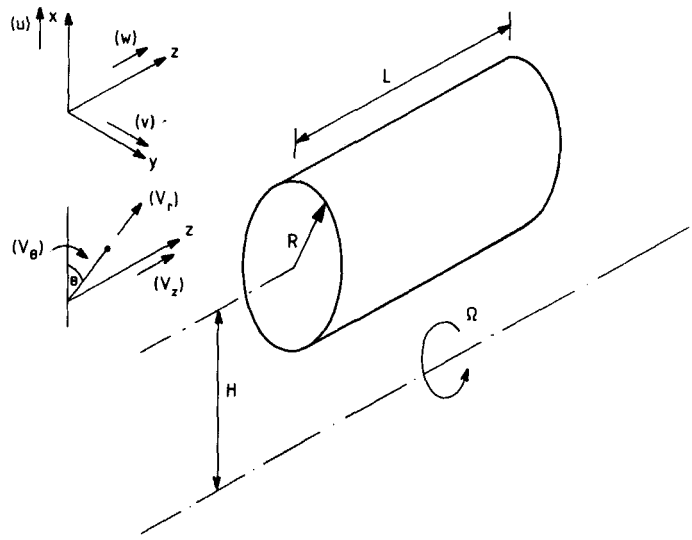

Figure 1. System nomeclature and geometry

$$\frac{Dw}{Dt} = F_z - \frac{1}{\rho}\frac{\partial p}{\partial z} + \nu\nabla^2 w. \tag{3}$$

The present analysis is addressed to steady operating conditions and therefore the total derivative terms (e.g. Du/Dt) contain convective elements only, i.e.

$$\frac{Du}{Dt} = u\frac{\partial u}{\partial x} + v\frac{\partial u}{\partial y} + w\frac{\partial u}{\partial z}.$$

Under such conditions the mass conservation equation may be expressed as

$$\frac{\partial u}{\partial x} + \frac{\partial v}{\partial y} + \frac{\partial w}{\partial z} = 0. \tag{4}$$

Equations (1)–(3) contain body force components F_x, F_y and F_z. For many flow problems these do not need to be considered; however, for the present problem the derivation in Reference 2 gives the result that

$$F_x = \Omega^2(H + x) + 2\Omega v, \tag{5}$$

$$F_y = \Omega^2 y - 2\Omega u, \tag{6}$$

while

$$F_z = 0. \tag{7}$$

Also it can be shown[4] that the terms $\Omega^2(H + x)$ and $\Omega^2 y$ only generate a hydrostatic head across the duct section and that, subject to ignoring any resulting density gradients across the pipe section, that is expected to have little or no effect on the flow behaviour existing in the duct. Indeed, in the turbogenerator the duct diameter is small in comparison with the eccentricity (H) and therefore any density variations are expected to be extremely small and may be safely ignored.

They the full momentum equations may be stated as

$$u\frac{\partial u}{\partial x}+v\frac{\partial u}{\partial y}+w\frac{\partial u}{\partial z}=-\frac{1}{\rho}\frac{\partial p}{\partial x}+2\Omega v+\nu\nabla^2 u, \tag{8}$$

$$u\frac{\partial v}{\partial x}+v\frac{\partial v}{\partial y}+w\frac{\partial v}{\partial z}=-\frac{1}{\rho}\frac{\partial p}{\partial y}-2\Omega u+\nu\nabla^2 v, \tag{9}$$

$$u\frac{\partial w}{\partial x}+v\frac{\partial w}{\partial y}+w\frac{\partial w}{\partial z}=-\frac{1}{\rho}\frac{\partial p}{\partial z}+\nu\nabla^2 w. \tag{10}$$

This equation set is highly non-linear; however, in the present study a solution was attempted using both finite difference and finite element methodology. For the finite difference analysis use was made of a computer code which is available commercially,[15] the requirement being to insert the pertinent body force (or inertial) contributions of equations (5) and (6).

In the finite element analysis the Galerkin weighted residual method was employed in conjunction with a mixed formulation as explained in Reference 12. At an element corner node this gives a nodal contribution to the overall stiffness matrix of the form

$$\begin{bmatrix} A_{11} & A_{12} & A_{13} & A_{14} \\ A_{21} & A_{22} & A_{23} & A_{24} \\ A_{31} & A_{32} & A_{33} & A_{34} \\ A_{41} & A_{42} & A_{43} & A_{44} \end{bmatrix} \begin{bmatrix} u \\ p \\ v \\ w \end{bmatrix} = \begin{bmatrix} B_1 \\ B_2 \\ B_3 \\ B_4 \end{bmatrix}. \tag{11}$$

The contributions to A_{11}, etc. are straightforward to determine; however, to enhance the convergence rate, the Newton–Raphson iteration algorithm was embodied. Also, since the elements used ensured inter-element continuity of value only (e.g. velocity) and not its derivative, it was necessary to reduce second-order derivatives using Green's theorem. The procedure is well documented; see, for example, Reference 16.

PROBLEM DISCRETIZATION, BOUNDARY CONDITIONS AND PRIMARY ANALYSIS

Initial analysis of the problem was carried out using the finite element method. A comparatively coarse three-dimensional weighted discretization comprising 280 20-node isoparametric brick elements[17] was used as shown in Figure 2. Boundary conditions were set to reflect non-slip at the physical boundaries (i.e. $u=v=w=0$), while at the inlet plane ($z/L=0{\cdot}0$) radial and azimuthal velocities were set to zero and the axial component assumed a uniform value over almost the entire face, a linear interpolation between the plane value and fixed boundary value being used at the near-wall element (see Figure 4 for the general form). At the downstream location, compatible with the observation in Reference 3, flow was assumed to be fully developed and utilization of the stress-type formulation obviated the need to prescribe pressure anywhere. After consideration of boundary conditions, the mesh shown in Figure 2 resulted in the need to solve 3423 equations simultaneously.

Calculation was carried out for a duct of radius (R) 7·0 mm and length (L) 623·0 mm fixed at an eccentricity (H) of 457·0 mm with a throughflow Reynolds number (Re) of 100 and a rotational Reynolds number (J) of 1384. This geometry was chosen to be compatible with that used in the experimental investigation described in Reference 3 so that where possible experimental and theoretical trends could be compared. Some results from this primary analysis are shown in Figure 3 in the form of streamlines in the duct section. These were obtained by postprocessing the

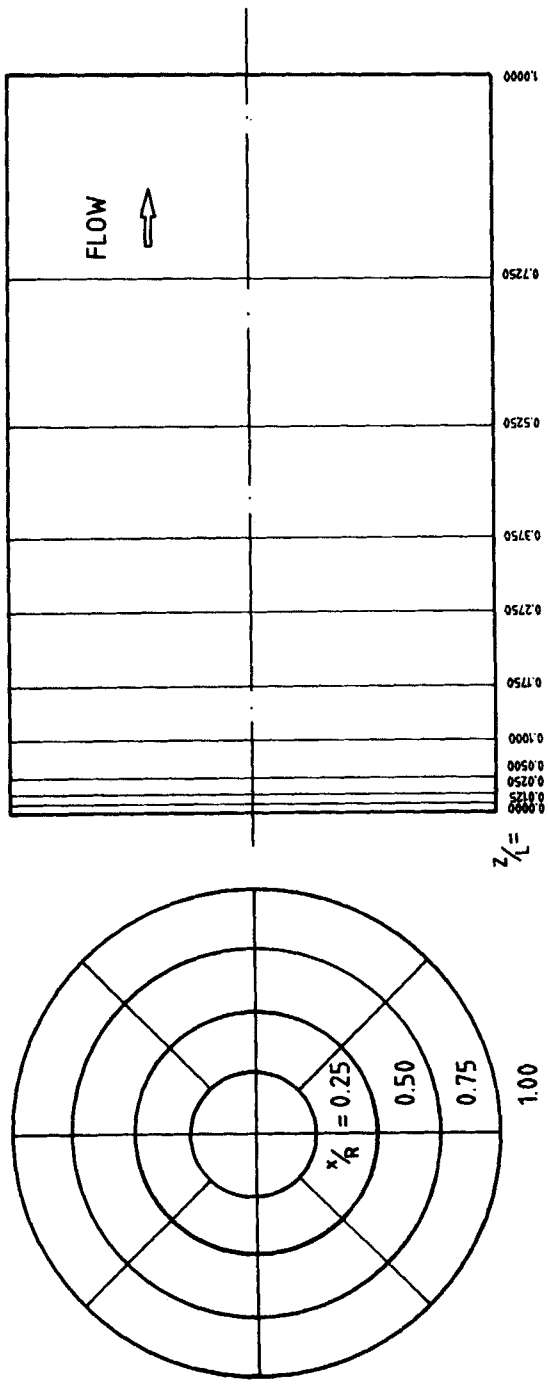

Figure 2. Elemental discretization—primary study

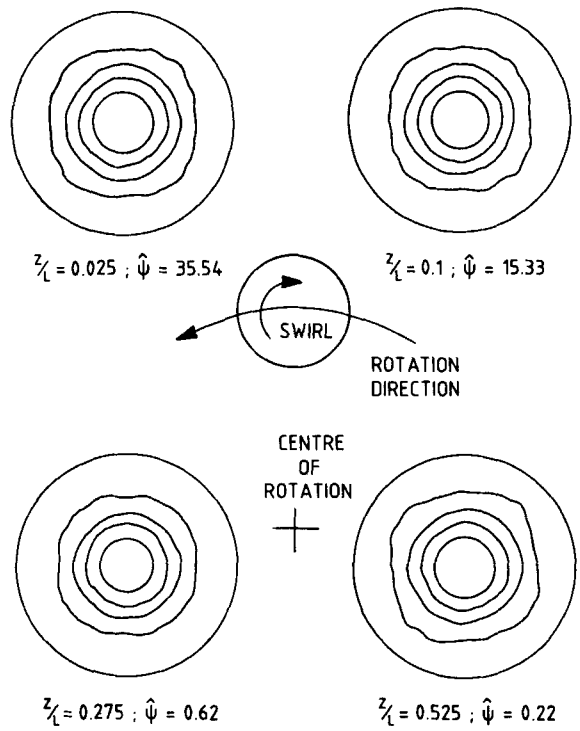

Figure 3. Circulation flow patterns at various streamwise locations; $R = 7{\cdot}0$ mm, $L = 623$ mm, $Re = 100$, $J = 1384$

velocity field data in the plane of the duct and plotting contours of constant streamfunction. These plots show quite clearly that the flow is swirling in form. The value of maximum streamfunction ($\hat{\psi}$) at the core suggests also that the circulation decays toward the outlet region of the pipe.

Such a circulatory flow is generated by the body force (or inertial) terms appearing in equations (8) and (9). In developing pipe flow it is well known that radially inward flow towards the pipe centre is induced near the entrance,[18] and when its components are introduced into the body force terms in the momentum equation (by the terms $2\Omega v$ and $2\Omega u$), it has the characteristic of a Coriolis component. This will then induce a circulatory flow pattern which is axisymmetric in nature. This is reflected in the general form of the flow patterns presented in Figure 3, where any departure from an axisymmetric form may be attributed to the coarseness of the element mesh. From a numerical analysis viewpoint this has very considerable implications, since now the governing equations can be simplified to take account of this. In a cylindrical co-ordinate system azimuthal velocity gradients vanish and the momentum equations become[14]

$$v_r \frac{\partial v_r}{\partial r} - \frac{v_\Phi^2}{r} + v_z \frac{\partial v_r}{\partial z} = -\frac{1}{\rho}\frac{\partial p}{\partial r} + 2\Omega v_\Phi + \nu\left[\nabla^2 v_r - \frac{v_r}{r^2}\right], \tag{12}$$

$$v_r \frac{\partial v_\Phi}{\partial r} + \frac{v_r v_\Phi}{r} + v_z \frac{\partial v_\Phi}{\partial z} = -2\Omega v_r + \nu\left[\nabla^2 v_\Phi - \frac{v_\Phi}{r}\right], \tag{13}$$

$$v_r \frac{\partial v_z}{\partial r} + v_2 \frac{\partial v_z}{\partial z} = -\frac{1}{\rho}\frac{\partial p}{\partial z} + \nu\nabla^2 v_z, \tag{14}$$

and the continuity equation becomes

$$\frac{\partial v_r}{\partial r}+\frac{v_r}{r}+\frac{\partial v_z}{\partial z}=0. \tag{15}$$

These equations may be discretized using the method explained in Reference 16 to yield either stress or gradient boundary conditions. However, it is now necessary to solve these equations in the r–z plane only. For the purpose of calculation stability, upwind weighting was included in the formulation as explained in Reference 19.

AXISYMMETRIC ANALYSIS

Detail considerations

As explained previously, both finite difference and finite element approaches were used to model the axisymmetric flow. Primary numerical experiments were carried out to determine the sensitivity of the solution to cell or mesh discretization. Initially this was carried out for the finite difference method, and during this part of the study it was found that to model the assumed downstream condition of developed flow it was necessary to extend the mesh to represent a pipe of length 1 m (as opposed to 0·623 m), since the velocity profiles were not fully developed at this latter location at the more extreme operating conditions. Using a process of trial and inspection, it was concluded that a mesh comprising 15 radial and 90 axial divisions gave a solution which was sufficiently independent of discretization. The grid is shown in Figure 4(a); note that every tenth plane is shown in the axial direction. Additionally the subdivision was weighted to give a fine discretization adjacent to the wall and at the inlet region to the pipe.

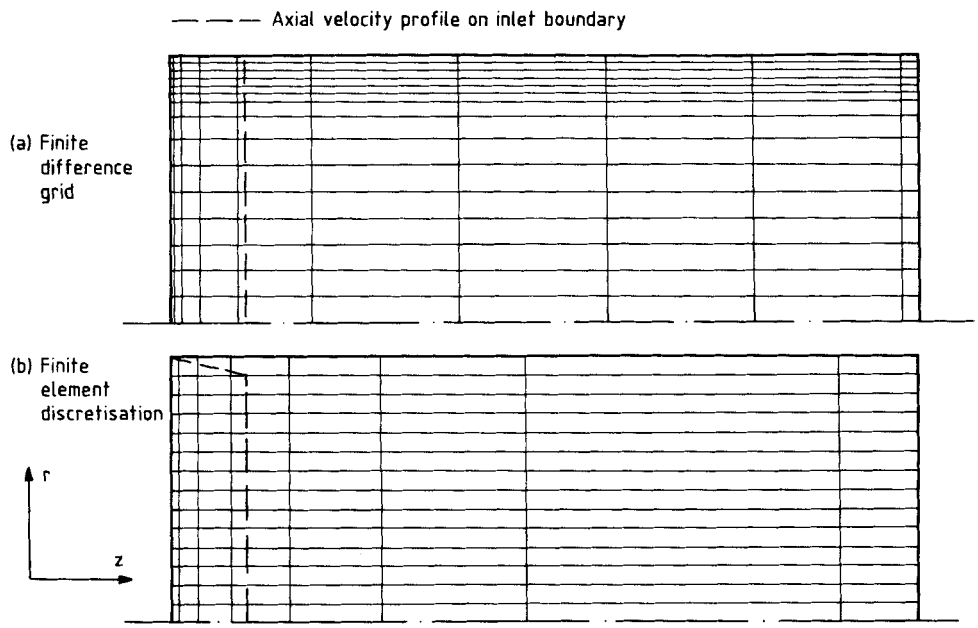

Figure 4. The final finite difference/element domain discretization

A similar process of assessing the sensitivity of the solution to mesh discretization was carried out for the finite element method. Additionally two formulation types were considered, the first to yield stress and the second to yield normal velocity gradients as the natural boundary conditions. Again, for convenience and to enable direct comparison, a pipe of 1 m length was used, although the finite element approach does enable developing flow boundary conditions to be dealt with as explained in Reference 20. Numerical experimentation suggested that a mesh comprising 14 radial and 30 axial divisions was adequate, with fine subdivision being employed in the inlet region and in the axial direction only. Figure 4(b) shows the discretization, where every fourth plane is shown in the axial direction.

Calculations were carried out for a throughflow Reynolds number (Re) of 500 and a rotational Reynolds number (J) of 400. Some detailed results from this analysis are shown in Figures 5–7. Figure 5(a) illustrates the variation of the predicted radial velocity field along the axis of the pipe at a given radial location using both of the numerical approaches. In both cases the analyses suggest that there is radial flow towards the pipe centreline which is very pronounced in the inlet region

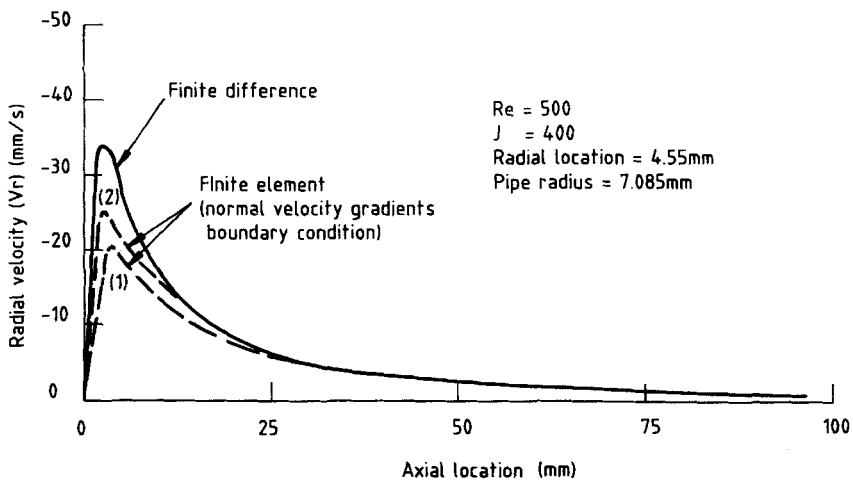

Figure 5(a). Variation of radial velocity with axial location near the pipe inlet

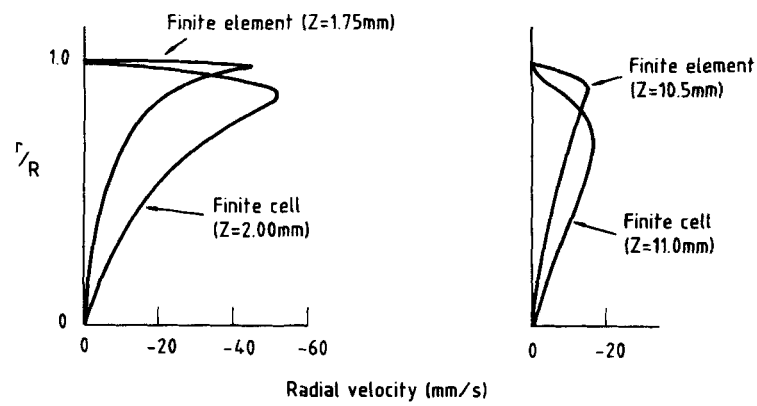

Figure 5(b). Radial velocity at different radial locations at the pipe inlet; $Re = 500$, $J = 400$, $R = 7{\cdot}085$ mm

(within the first 25 mm). Additionally it can be seen that there is some difference in the predicted magnitude using both methods, the finite difference method giving the higher value. This may be attributed in part to the nature of the inlet boundary condition employed in the finite element method. In the figure, two curves are illustrated for this analytical approach. Curve 1 corresponds to the boundary condition where the inlet plane velocity is interpolated to zero over the near-wall element (see Figure 4) and curve 2 where the inlet velocity is truly plain. The latter approximates most closely that employed in the finite cell analysis and which, as a consequence, gives the closest agreement with it.

Figure 5(b) illustrates the radial variation of radial velocity in the pipe inlet region for both numerical schemes. The two approaches show noticeable differences: for the finite element scheme the radially inward flow is confined to an area close to the pipe wall, whereas for the finite cell method the radial inflow is significant over a larger section of the pipe. This difference in radial velocity profiles is reflected clearly in the nature and extent of the swirling flow patterns shown in Figure 6.

Figure 6(a) illustrates the variation of the azimuthal velocity component at a fixed radial location over the pipe length. From this it can be seen that there is considerable swirling motion, particularly near the pipe inlet. However, the magnitude of the swirling motion is dependent on the numerical procedure adopted. The finite cell method predicts the most vigorous activity which extends over a significant length of the pipe, and this is compatible with the higher radial velocities and radial change in radial velocity shown in Figure 5. For the finite element results in Figure 6(a) the effect of using two inlet boundary conditions is shown (curves 1 and 2) and these correspond to those discussed for Figure 5. The figure also shows the result of using a stress-type formulation and this clearly illustrates a reduced circulatory motion, although for this latter analysis the downstream boundary conditions were not updated using the method described in Reference 20. Additionally it can be seen that the swirling motion is in the opposite direction to pipe rotation when viewed from the inlet end; this is compatible with the Coriolis driving mechanism involved (see Figure 3 also).

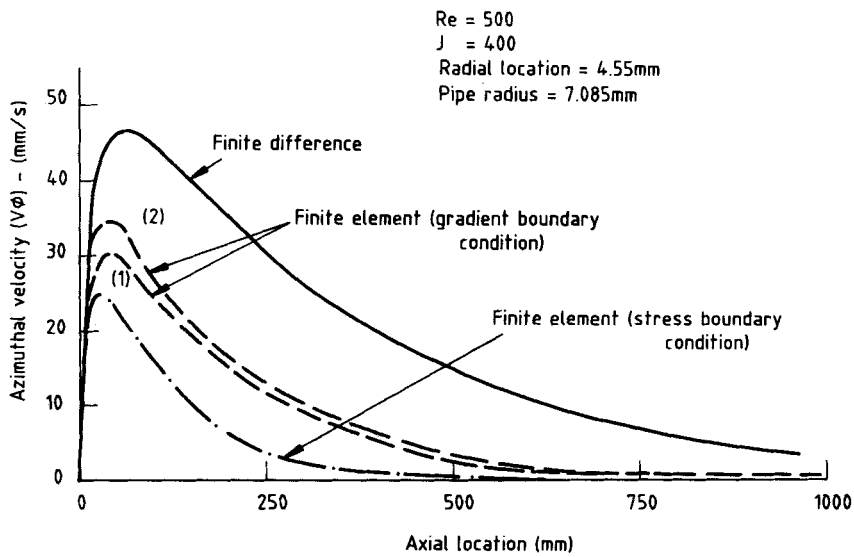

Figure 6(a). Variation of azimuthal velocity with axial location

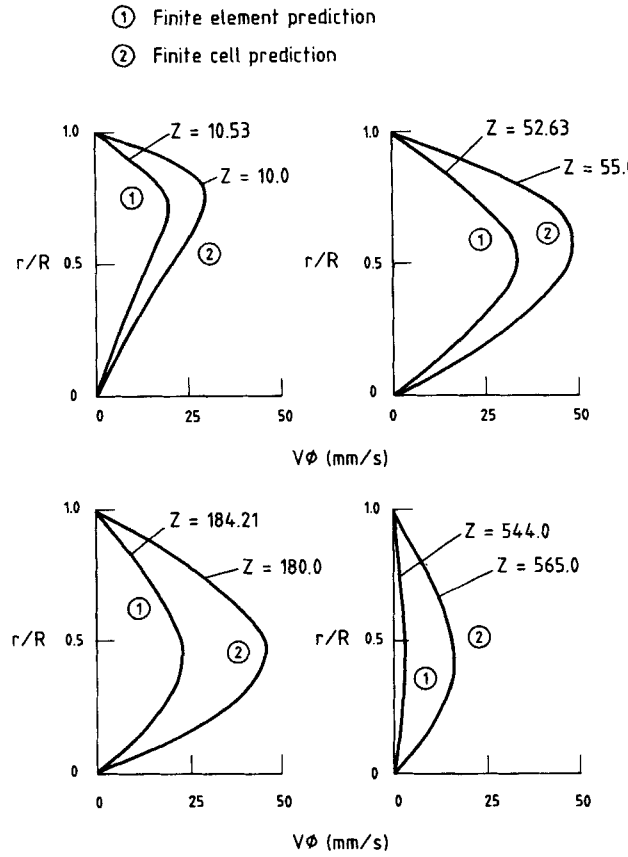

Figure 6(b). Comparison of azimuthal velocity components at various axial locations; $Re = 500$, $J = 400$

The variation of azimuthal velocity with radial location is shown for four axial locations in Figure 6(b). Close to the pipe inlet (about 10 mm downstream) the velocity profile suggests that there is a central core (up to $r/R = 0{\cdot}7$) which is subject to solid body rotation with high shearing close to the pipe wall. Further downstream, however, the maximum swirl velocity occurs nearly halfway between the centreline and the wall. From Figure 6 it is clear that the two numerical methods predict flow patterns where the magnitude of the swirl action is different. The finite cell method suggests that even when the radially inward flow which is responsible for the swirl action is confined to a small section close to the pipe inlet, the flow circulates for a long distance downstream. Conversely, the finite element method indicates that the circulatory flow is not so strong and does not extend so far downstream. However, there is no experimental evidence to confirm the accuracy of either method for the flow configuration under consideration.

Figure 7 illustrates the near-wall axial pressure profile predicted using both numerical techniques. Additionally the figure includes that from a closed-form solution for fully developed pipe flow which may be used to provide a useful datum for comparison. In the developed flow region the pressure gradient which may be deduced from either numerical result does not agree precisely with that obtained from the closed-form solution. However, marginally better agreement was obtained from the finite element solution for a stationary pipe. Additionally neither numerical method predicted significant changes in the axial pressure field when the pipe was either stationary

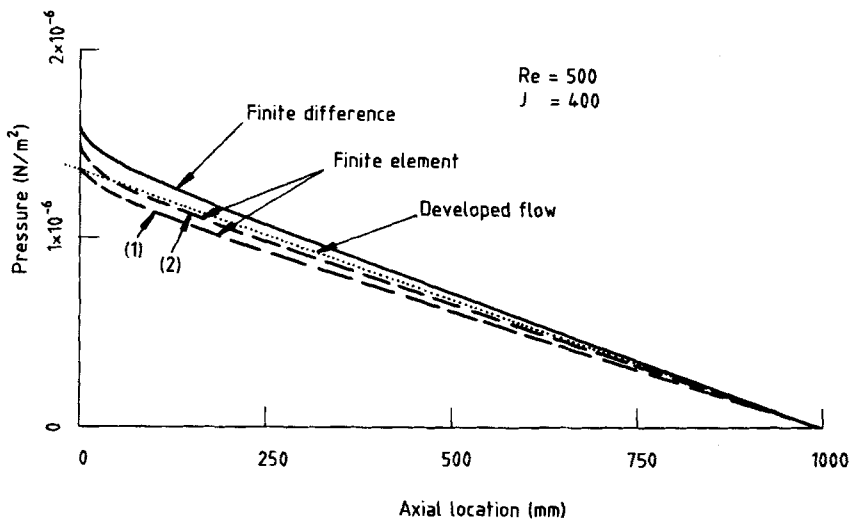

Figure 7. Axial pressure variation at the pipe wall

or rotating. This is in some conflict with the experimental data presented in Reference 3, but in this work it was shown that the friction factor (or pressure gradient indirectly) was dependent on the inlet configuration which must therefore affect the nature of the flow into the experimental section. Such minor changes in predicted pressure drop for both stationary and rotating ducts may be anticipated, since the azimuthal velocity component is weakly linked into the radial momentum equation only (i.e. equation (12)). It is not present in the axial momentum equation which has the dominant influence on the axial pressure gradient.

Global analysis

Figure 8 illustrates the results from a series of calculations to investigate the effect of varying both throughflow and rotational speed on the magnitude of the swirl. For these calculations the axial velocity profile at the pipe inflow plane was assumed to be plain in the centre with linear interpolation to zero over the near-wall element.

Figure 8(a) shows the effect of varying rotational speed for a fixed throughflow Reynolds number. From these curves it is evident that the magnitude of the swirl increases linearly with the rotational speed. It may be noted also that the position of the peak swirl velocity depends on the axial position; however, in all cases it occurs at the same radial location.

The behaviour where different throughflow Reynolds number effects are investigated is shown in Figure 8(b). These results show that the magnitude of the swirl component varies in a complex manner. Close to the pipe inlet the magnitude of the swirl component is greatest for the lowest throughflow Reynolds number. This is a surprising result since the radial velocity component is smallest for this condition (see Figure 9(a)). Nearly the same condition prevails at the next axial location, while at the third axial location ($z = 184$ mm) the case where the throughflow velocity is highest gives the strongest swirling motion. This prevails to the pipe outlet where considerable swirl persists for the highest throughflow velocity. The results in Figure 8 suggest therefore that the position of maximum swirl depends on the flow rate of fluid through the duct and this is shown in Figure 9.

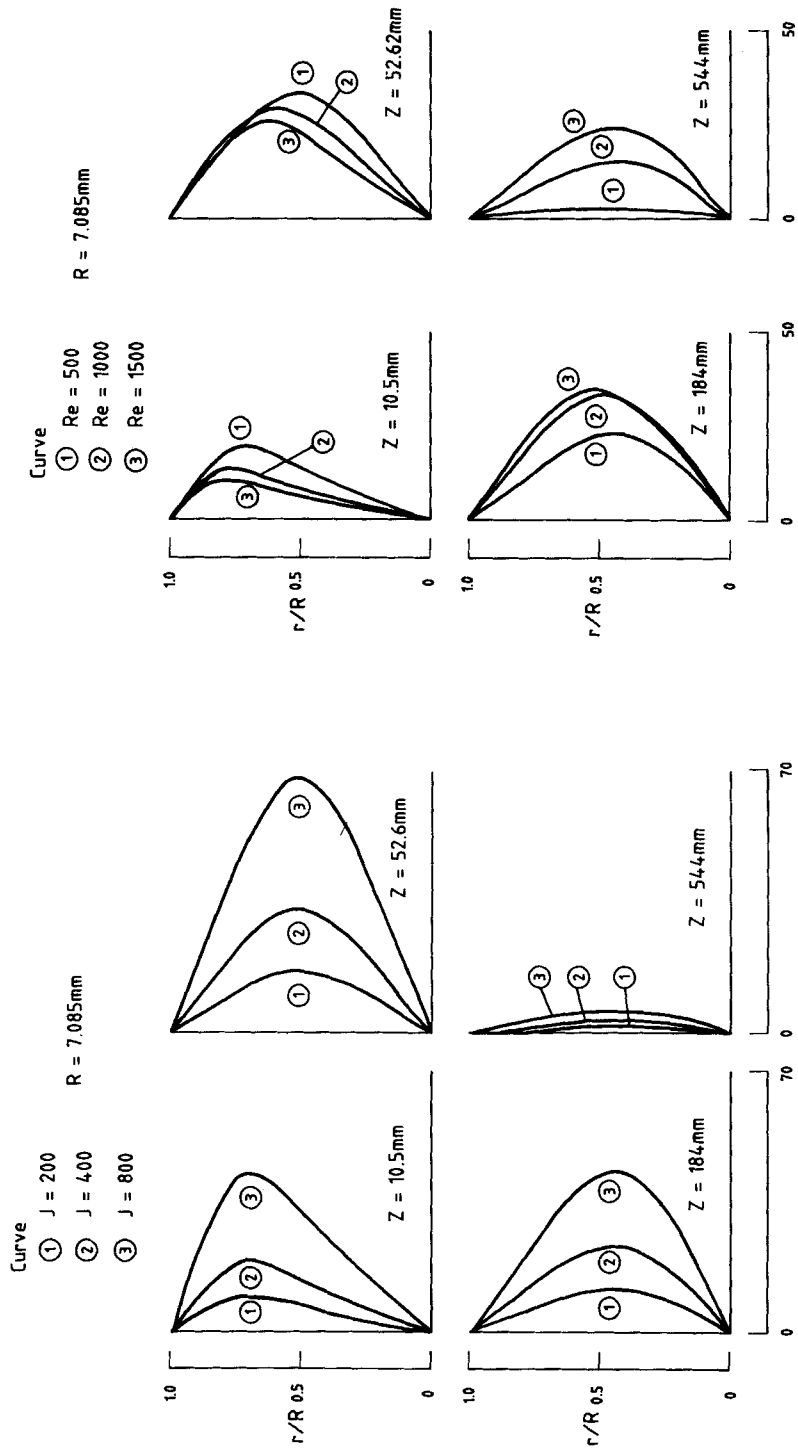

Figure 8(a). Azimuthal velocity profiles at different axial locations and rotational speed; $Re = 500$

Figure 8(b). Azimuthal velocity profiles at various axial stations and throughflow Reynolds number; $J = 400$

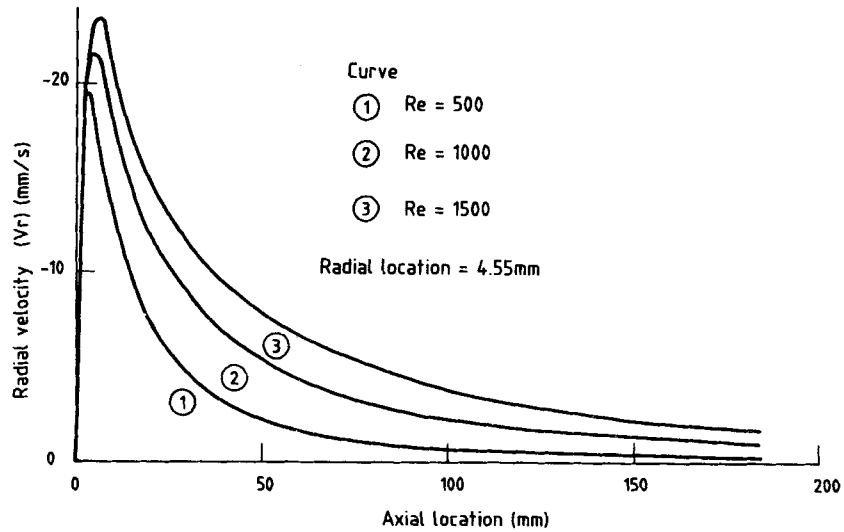

Figure 9(a). Radial velocity in the pipe inlet region for different throughflow Reynolds number; $J = 400$

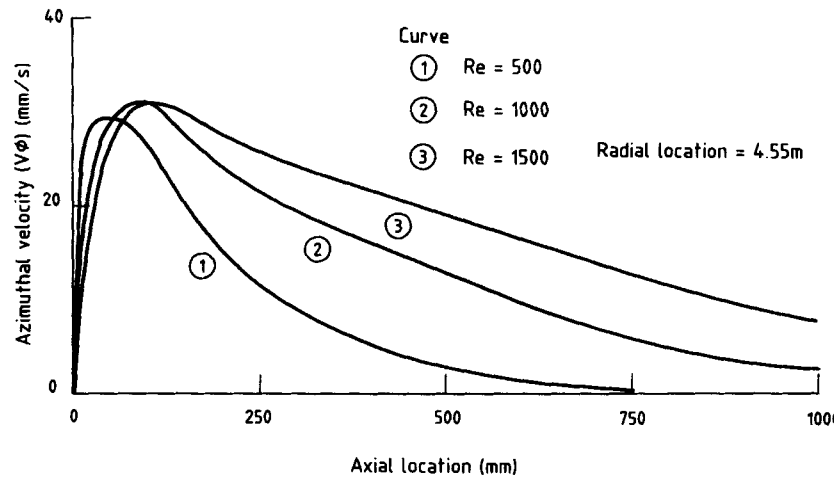

Figure 9(b). Azimuthal velocity over the pipe length for various throughflows; $J = 400$

Radial velocity profiles over the pipe length are shown in Figure 9(a), and their variation has been presented since these provide the motivation for the swirl action. As expected, the magnitude of the radially inward velocity increases with throughflow Reynolds number. The resulting swirl is shown in Figure 9(b) and it is clear that the different flow rates result in different swirl patterns. The analysis suggests that despite the different radial velocities the magnitude of the peak swirl does not differ significantly; however, for the higher throughflow, swirling action persists much further down the pipe since active radial flow occurs over a longer distance and thereby energizes it.

Numerical efficiency

The solution of the same problem on the same computer enabled a direct comparison of the efficiency of the two numerical techniques. For the finite cell analysis the grid comprised 1350 cells and therefore 5400 equations were solved to yield the three velocity components and the pressure field. The resulting equation set is tridiagonal in nature[10] and this is amenable to very rapid solution. For the finite element analyses there was a requirement to solve for 4132 unknown variables and this was achieved by adopting a Gaussian-elimination-type method.[12] For the finite cell method a complete solution was obtained in about 88 min, while for the finite element method, based on the need for seven iterations to achieve convergence (at 900 s/iteration), the time required was 105 min. This suggests that the finite cell method is more efficient and this arises from the tridiagonal nature of the equations. Some improvement in the efficiency of the finite element approach may be achieved by decoupling the solution of the azimuthal momentum equation. This is probably feasible since it contains velocity terms only, and its decoupling will result in a more closely banded matrix which will be solved more efficiently by the Gaussian elimination algorithm.

CONCLUSIONS

A finite element and finite cell analysis of flow in a circular duct rotating about an axis parallel to its own has been presented. The following conclusions can be drawn from this work.

1. The combined rotation and radial flow in the pipe inlet produces a swirling flow pattern in the pipe which is opposite in direction to that of pipe rotation when viewed from the inlet end. This is due to the introduction of a Coriolis-type term into the azimuthal and radial momentum equations.
2. The strength of the swirling motion depends on and is proportional to the rotational speed, while its extent depends on the flow rate through the tube. At the higher throughflow the swirl is least significant near the pipe inlet but becomes more important further downstream, a trend which is reversed at the lower flow rates. This is due to the different magnitude of the radially inward velocities for the different conditions.
3. For the finite element solution the normal velocity gradient formulation gives the closest agreement with the finite cell analysis. Also the strength of the swirling motion depends on the shape of the inlet velocity profiles, the closest agreement between numerical methods being achieved when the shapes agree most closely. Confirmation of this sensitivity to inlet conditions is provided by experimentally measured pressure drops.

APPENDIX: NOMENCLATURE

F_x, F_y, F_z	body force terms in equations (1)–(3)
H	pipe eccentricity (see Figure 1)
J	rotational Reynolds number ($=\Omega d^2/\nu$)
L	pipe length
R	pipe radius
Re	throughflow Reynolds number ($=Ud/\nu$)
U	mean axial velocity
d	pipe diameter
p	pressure
r, z, Φ	co-ordinate directions (cylindrical)

t	time
u, v, w	velocity components (Cartesian axes)
v_r, v_Φ, v_z	velocity components (cylindrical system)
x, y, z	co-ordinate directions (Cartesian)
ψ	streamfunction
Ω	angular velocity (rad s^{-1})
ν	fluid kinematic viscosity
ρ	fluid density

REFERENCES

1. B. A. Marlow, 'The mechanical design of large turbogenerators', *Proc. I Mech. E*, **200**, 1–13 (1986).
2. W. D. Morris, *Heat Transfer and Fluid Flow in Rotating Coolant Channels*, Research Studies Press (John Wiley), 1981.
3. A. R. Johnson and W. D. Morris, 'Experimental investigation of the effect of entry conditions and rotation on flow resistance in circular tubes rotating about a parallel axis', *Int. J. Heat Fluid Flow*, **5**, 121 (1984).
4. W. D. Morris, 'The influence of rotation on flow in a tube rotating about a parallel axis with uniform angular velocity, *J. Roy. Aeronaut. Soc.* **69**, 201 (1965).
5. J. L. Woods and W. D. Morris, 'An investigation of laminar flow in the rotor windings of directly cooled electrical machines', *J. Mech. Eng. Sci.*, **16**, 408 (1974).
6. Y. Mori and W. Nakayama, 'Forced convective heat transfer in a straight pipe rotating about a parallel axis (laminar region)', *Int. J. Heat Mass Transfer*, **10**, 1179 (1967).
7. D. Skiadaressis and D. B. Spalding, 'Laminar heat transfer in a pipe rotating about a parallel axis', *Imperial College of Science and Technology Mechanical Engineering Report No. HTS/76/23*, 1976.
8. L. Talbot, 'Laminar swirling pipe flow', *J. Appl. Mech.* **21**, 1 (1954).
9. E. M. Sparrow and A. Chaboki, 'Swirl-affected turbulent fluid flow and heat transfer in a circular tube', *Trans. ASME, J. Heat Transfer*, **106**, 766 (1984).
10. D. B. Spalding, 'A novel finite difference formulation for differential equations involving both first and second derivatives', *Int. j. numer. methods eng.* **4**, 551 (1972).
11. C. Taylor and P. Hood, 'A numerical solution of the Navier–Stokes equations using the finite element technique', *Comput. Fluids*, **1**, 73 (1973).
12. P. Hood and C. Taylor, 'Navier–Stokes equations using mixed interpolation', J. T. Oden *et al.* (eds), *Finite Element Method in Flow Problems*, 1974.
13. R. M. Smith, 'A practical method of two equation turbulence modelling using finite elements', *Int. j. numer. methods fluids*, **4**, 321–336 (1984).
14. H. Schlichting, *Boundary Layer Theory*, Pergamon Press, 1955.
15. *PHOENICS User Manual*, Concentration Heat And Momentum Ltd., (CHAM) Bakery House, 40 High Street, Wimbledon, London.
16. C. Taylor and T. G. Hughes, *Finite Element Programming of the Navier–Stokes Equations*, Pineridge Press, 1981.
17. O. C. Zienkiewicz, *The Finite Element Method*, McGraw-Hill, 1977.
18. A. Z. Ijam, 'Finite elements in incompressible viscous flow including heat transfer', *Ph.D. Thesis*, University College of Wales, Swanesea, 1977.
19. P. Bar Yoseph, J. J. Blech and A. Solan, 'Upwind schemes for the finite element solution of the Navier–Stokes equation in rotating flows', in C. Taylor *et al.* (eds), *Proc. Int. Conf. on Numerical Methods in Laminar and Turbulent Flows*, 1978.
20. C. Taylor, J. Rance and J. O. Medwell, 'Note on the imposition of traction boundary conditions when using the FEM for solving incompressible flow problems', *Commun. Appl. Numer. Methods*, **1**, 113–121 (1985).